On the X-ray Variability and Disk Truncation in Dwarf Novae

ŞÖLEN BALMAN

Department of Physics, Middle East Technical University, Ankara, 06531, Turkey

Details of this study are in **Balman** & **Revnivtsev 2012, A&A, 546, 112**

SUMMARY

We perform power spectral analysis of the X-ray light curves obtained using the Rossi X-ray Timing Explorer (*RXTE*) and X-ray Multi-mirror Mission (*XMM-Newton*) data. In addition, we apply cross-correlation analysis of simultaneous UV and X-ray light curves using the *XMM-Newton* data to determine time lags between the different wavelength data. For five dwarf nova (DN) systems, SS Cyg, VW Hyi, RU Peg, WW Cet, and T Leo we show that the UV and X-ray power spectra of their time variable light curves are similar in quiescence. All of them show a break in their power spectra, which in the framework of the model of propagating fluctuations indicates inner disk truncation. We derive the inner disk radii for these systems in a range (10-3)$\times 10^9$ cm. We analyze the *RXTE* data of SS Cyg in outburst and compare it with the power spectra, obtained during the period of quiescence. We show that during the outburst the disk moves towards the white dwarf and recedes as the outburst declines. We calculate the correlation between the simultaneous UV and X-ray light curves of the five DN studied in this work, using the *XMM-Newton* data obtained in the quiescence and find X-ray time lags of 96-181 sec. This can be explained by the travel time of matter from a truncated inner disk to the white dwarf surface. We suggest that, in general, DN may have truncated accretion disks in quiescence which can also explain the UV and X-ray delays in the outburst stage and that the accretion may occur through coronal flows in the disk (e.g., rotating accretion disk coronae). Within the framework of the model of propagating fluctuations, the comparison of the X-ray/UV time lags observed by us in the case of DN systems with those detected for a magnetic intermediate polar allows us to make a rough estimate of the viscosity parameter $\alpha \sim 0.25$ in the innermost parts of the accretion flow of DN systems.

1 Introduction

Cataclysmic variables (CVs) are interacting binaries hosting a white dwarf (WD) primary star accreting material from a late-type main sequence star. Accreting material forms a disk that is expected to reach all the way to the WD in cases where the magnetic field of the WD is weak ($B < 0.01$ MG) and these systems are referred to as nonmagnetic CVs (see Warner 1995 for a review). In our work we consider dwarf novae (DNe), a subclass of nonmagnetic cataclysmic variables.

The truncation of the optically thick accretion disk in DNe in quiescence was observationally invoked due to the observed time lags between the optical and UV fluxes in the rise phase of the outbursts (Ladota 2001, 2004) or due to unusual shape of the optical spectra or light curves of DNe (Linell et al. 2005, Kuulkers et al. 2011). Theoretical support for such a two-phase flow was given by a model of the disk evaporation of (Meyer & Meyer-Hofmeister 1994). This model was later elaborated to show that the disk evaporation (coronal "syphon" flow) may create optically thick-optically thin transition regions at various distances from the WD (Liu et al. 1997, Mineshige et al. 1998). Recently, an additional diagnostic tool has been proposed - the aperiodic variability of brightness of sources. While the long time-scale variability might be created in the outer parts of the accretion disk (Warner & Nather 1971), the relatively fast time variability (at f >few mHz) originates in the inner parts of the accretion flow (Bruch 1992,2000; Baptista & Borteletto 2004).

Properties of this noise is similar to that of the X-ray binaries with neutron stars and black holes. Now, the widely accepted model of origin for this aperiodic flicker noise is a model of propagating fluctuations (Lyubarskii 1997, Churazov et al. 2001, Uttley & McHardy 2001, Revnivtsev et al. 2009,2010, Uttlet et al. 2011). The modulations of the light are created by variations in the instantaneous value of the mass accretion rate in the region of the energy release. These variations in the mass accretion rate, in turn, are inserted into the flow at all radii of the accretion disk due to the stochastic nature of its viscosity and then transferred toward the compact object.

This model predicts that the truncated accretion disk should lack some part of its variability at high Fourier frequencies, i.e. on the time scales shorter than a typical time scale of variability. In this paper we would like to apply the similar diagnostic tool to estimate the inner boundary of the optically thick accretion disk in nonmagnetic WDs – dwarf novae.

2 The Data and the Observation

The power spectral densities (PDS) expressed were calculated in terms of the fractional rms amplitude squared following from (Miyamoto et al. 1991),

$$P_j = 2|A_j|^2/N_{ph}C \qquad A_j = \sum x_n e^{i\omega_n t_n}$$

. In this prescription, t_n is the time label for each time bin, x_n is the number of counts in these bins, N_{ph} the total number of photons in each light curve, and C the average count rate in each time segment used to construct PSD. The white noise levels were subtracted hence leaving us with the rms fractional variability of the time series in units of $(\mathrm{rms/mean})^2$/Hz. Next, we multiplied the rms fractional variability per hertz with the frequencies at which they were calculated to yield an rms fractional variability squared, thus our PDS are νP_ν versus ν. For the model fitting we used a simple analytical model

$$P(\nu) \propto \nu^{-1}\left(1+\left(\frac{\nu}{\nu_0}\right)^4\right)^{-1/4}$$

,
which was proposed to describe the power spectra of sources with truncated accretion disks (see Revnivtsev et al. 2010,2011).

Table 1: The log of observations (list of Observation IDs) used in our work. All *RXTE* data is of SS Cyg.

RXTE Quiescence	20033013100–14200, 50011018000–19700, 50012010101–10109
RXTE X-ray dips	40012010200, 50011013100–14300, 95421010800, 95421011000, 954210200–204
RXTE X-ray Peak	40012011100–11800, 50011015800–17100, 95421010300–10301, 50012010104–10108
XMM-Newton Quiescence	0111970301 (VW Hyi), 0111970901 (WW Cet), 0551920101 (RU Peg), 0111970701 (T Leo)

3 SS Cyg Power Spectra

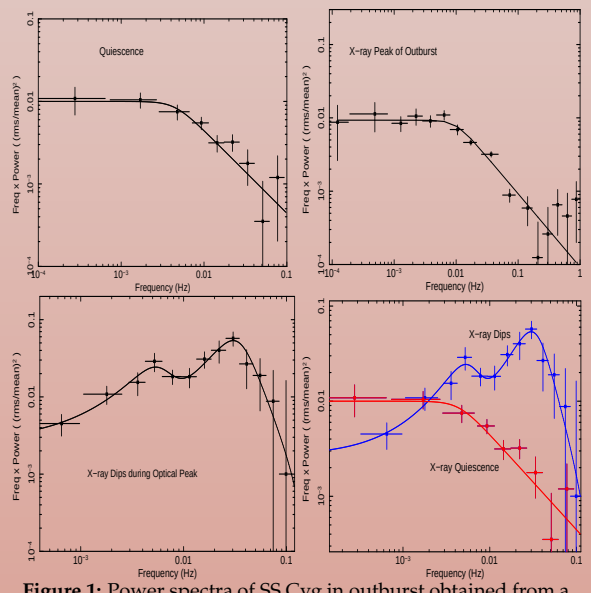

Figure 1: Power spectra of SS Cyg in outburst obtained from a collection of archival *RXTE* data listed in Table 1. The PDS at different times are ordered as the quiesence on the top lefthand side, the X-ray peak on the top righthand side, and the X-ray dips during the optical peak on the bottom lefthand side. On the bottom righthand side, the PDS of SS Cyg in quiescence and during the X-ray suppression (optical peak) is shown for comparison. The solid lines show the fit with the propagating fluctuations model for the top figures and for the PDS of the X-ray dips two Lorentzians along with the propagating fluctuations model are used to achieve the best fitting results. The reduced χ^2values of the fits are 0.62, 1.5, and 0.4 for the quiescence, the X-ray peak and the X-ray dips, respectively.

4 WW Cet and T Leo

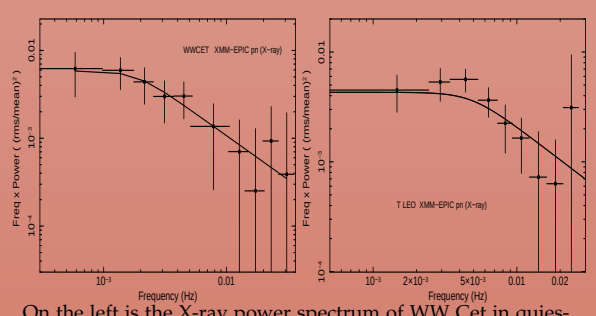

On the left is the X-ray power spectrum of WW Cet in quiescence obtained from the *XMM-Newton* EPIC pn data. Overplotted is the fitted curve using the the propagating fluctuations model. The reduced $\chi^2$of the fit to the *XMM-Newton* (EPIC pn) PDS is 0.2 . On the right is the power spectrum of T Leo in quiescence obtained from the *XMM-Newton* EPIC pn data. Overplotted is the fitted curve using the power relation for the noise from the propagating fluctuations model. The reduced $\chi^2$of the fit to the *XMM-Newton* (EPIC pn) PDS is 0.7 .

5 RU Peg and VW Hyi

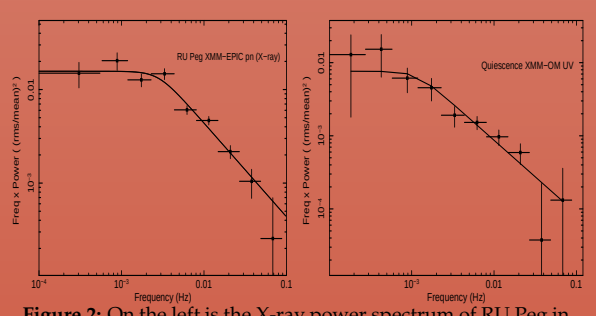

Figure 2: On the left is the X-ray power spectrum of RU Peg in quiescence obtained from the *XMM-Newton* EPIC pn data. Black solid line is the fitted curve using the propagating fluctuations model. The reduced $\chi^2$of the fit to the *XMM-Newton* (EPIC pn) PDS is 1.5 . On the right is the UV power spectrum of RU Peg in quiescence obtained from the *XMM-Newton* OM data. Black solid line is the fitted curve using the propagating fluctuations model. The reduced $\chi^2$of the fit to the *XMM-Newton* (OM) PDS is 0.8 .

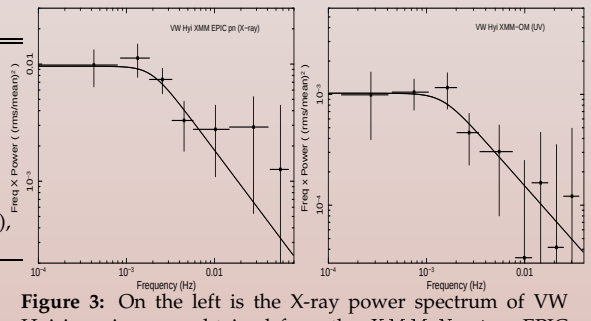

Figure 3: On the left is the X-ray power spectrum of VW Hyi in quiescence obtained from the *XMM-Newton* EPIC data. Overplotted curve is the fitted propagating fluctuations model. The reduced $\chi^2$of the fit to the *XMM-Newton* (EPIC pn) PDS is 0.5 . On the right is the UV power spectrum of VW Hyi in quiescence obtained from the *XMM-Newton* OM data. Overplotted curve is the fitted propagating fluctuations model. The reduced $\chi^2$of the fit to the *XMM-Newton* (OM) PDS is 0.4 .

6 The cross-correlations

The optical/UV light variations, generated as an energy release of variable mass accretion rate at the inner edge of the accretion disk, should lead the X-ray emission with the time lag equal to the time needed for the matter to travel from the inner edge of the disk to the central regions of the accretion flow in the vicinity of the WD, where the bulk of the X-ray emission is generated.

To study this question, we calculated the cross-correlation between the two simultaneous light curves (X-ray and UV), using the archival *XMM-Newton* data utilizing HEASOFT task CROSSCOR. To obtain the CCFs (cross-correlation functions), we divided our datasets into several pieces using 1-5 sec binning in light curves and calculated CCFs for each of them and fitted the resulting CCFs with double Lorentzians since it was necessary for adequate fitting.

The curves for all the DNe show clear asymmetry indicating that some part of the UV flux is leading the X-ray flux. In addition, we detect a strong peak near zero time lag for RU Peg, WW Cet and T Leo, suggesting a significant zero-lag correlation between the X-rays and the UV light curves.

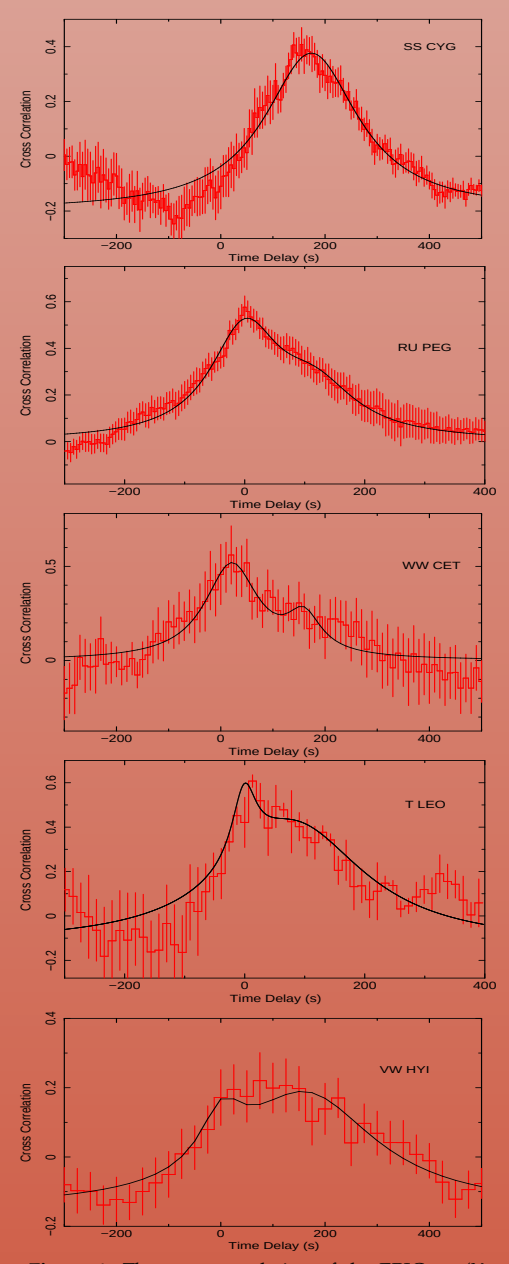

Figure 4: The cross-correlation of the EPIC pn (X-ray) and OM (UV) light curves with 1 sec time resolution. The CCFs are displayed for SS Cyg, RU Peg, WW Cet, T Leo, and VW Hyi from the top to the bottom of the figure. The correlation coefficient is normalized to a maximum value of 1. The error bars are evaluated as root mean square deviations from the average value of the cross-corelation of each measurement (made by using the segments of the whole light curve). The two-component Lorenzian fits are shown as solid black lines (except for SS Cyg where a single Lorentzian was used). The reduced χ^2values are 0.8, 0.4, 0.45, 1.2, and 0.45 from the top to the bottom panels of the figure.

Table 2: The break frequencies, disk truncation radii, and time delays of the dwarf novae analyzed in this work.

Source	State	Break Freq. (mHz)
SS Cyg	(quiescence-XMM)	5.6±1.4
SS Cyg	(quiescence-RXTE)	4.5±1.3
SS Cyg	(X-ray Dips)	50.0±20.0
SS Cyg	(X-ray peak)	9.7±1.5
RU Peg	(quiescence)	2.8±0.5
VW Hyi	(quiescence)	2.0±0.6
WW Cet	(quiescence)	3.0±1.7
T Leo	(quiescence)	4.5±1.5
Radius ($\times 10^9$ cm)	**Delay (s)**	**Log(L_{UVW1}/L_X)**
4.8±1.2	166-181 (χ^2_ν=0.8)	-4.3
5.5±1.8		
1.1±0.5		
3.3±0.5		
8.2±1.5	97-109 (χ^2_ν=1.7)	-3.1
8.1±2.5	103-165 (χ^2_ν=0.5)	-2.7
6.8±3.8	118-136 (χ^2_ν=1.6)	-3.6
4.0±1.3	96-121 (χ^2_ν=1.4)	-3.7

Notes. The last column is the logarithm of the ratio between the UV and X-ray luminosities. The UV Luminosities are in erg s^{-1} $Å^{-1}$ obtained using the *XMM-Newton* OM UVW1 (240-340 nm) filter. The errors represent 90 % confidence level. The χ^2_νvalues are for the delays calculated from fits with the subtracted CCFs except for SS Cyg for which a single Lorentzian fit was applied.

To double-check the two-Lorentzian fits, we constructed a more physically motivated plot of time-correlation using the shape of the auto-correlation of the X-ray light curves. Assuming that the zero time-lag signal on the original cross-correlation plot is created by a simple transformation of the X-ray variability into the UV light, we subtracted that part adopting the shape of X-ray auto-correlation function. The amplitude of this zero time-lag component was taken to provide smooth behavior of the subtracted cross-correlation function across zero delay. The subtracted cross-correlation functions directly yield the shifted time-lag component see the Figure 5 below.

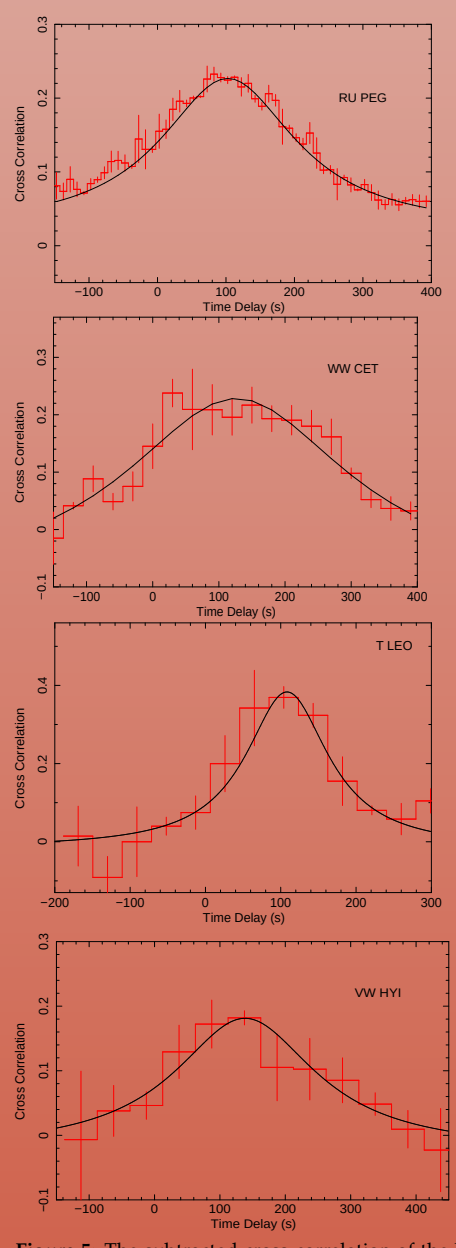

Figure 5: The subtracted cross-correlation of the EPIC pn (X-ray) and OM (UV) light curves (see the text for details). The residuals of the fits to the cross-correlations are displayed for RU Peg, WW Cet, T Leo, and VW Hyi from the top to the bottom of the figure. Single Lorenzian fits applied are shown as solid black lines (SS Cyg has been excluded since only a single Lorentzian was already used). The reduced χ^2values of the fits are given in Table 2.